Journal Homepage: http://ijcpe.uobaghdad.edu.iq
Iraqi Journal of Chemical and Petroleum Engineering
Vol. 27 No. 1 (March 2026) 117 – 126
EISSN: 2618-0707, PISSN: 1997-4884

Adsorption of methyl violet dye using MgO nanoparticles: Synthesis and kinetics

Mohammed Y. Eisa [a, *], Mariam Saleh Almufti [a]

a Biochemical Engineering Department, Al-Khwarizmi College of Engineering, University of Baghdad, Baghdad, Iraq

Abstract

A scalable method of oxalate co-precipitation was used to prepare magnesium oxide (MgO) nanoparticles. The precipitant used was oxalic acid and the source of soluble magnesium was magnesium sulfate. Highly crystalline MgO nanoparticles prepared by calcining at 700℃ were characterized by X-ray diffraction (XRD), scanning electron microscopy (SEM) and Atomic Force Microcopy Analysis (AFM). The (MgO) nanoparticles were employed to investigate the adsorption performance of Methyl Violet (MV) dye from aqueous solutions under different conditions, i.e., contact time, pH, dye concentration and temperature. Maximum adsorption (96%) was obtained at time (60 min.), pH 6, at (20℃) and adsorbent dosage (0.05 g/L). It was found that the effect of temperature is inversely proportional to the percentage of dye removal in the studied range (20-50℃). Pseudo-second-order (R^2=0.9968) and Langmuir models (R^2=0.9931) described excellent fits in kinetic and isotherm experiments, respectively, indicating monolayer coverage and chemisorption. The greater adsorption capability of MgO was verified in comparison to equivalent adsorbents (qmax=83.1 mg/g).

Keywords: Magnesium Oxide Nanoparticles; Methyl Violet Dye; Adsorption Isotherm; Adsorption kinetics.

Received on 26/10/2025, Received in Revised Form on 02/01/2026, Accepted on 03/01/2026, Published on 30/03/2026

https://doi.org/10.31699/IJCPE.2026.1.10

1- Introduction

Synthetic dyes have become a growing environmental concern, being a significant source of water pollution, due to their extensive use in many industries such as textiles, paper, cosmetics, and pharmaceuticals. These dyes pose serious ecological and health hazards, in addition to degrading the aesthetic qualities of water bodies [1].
One of the main ecological issues with such contamination is the interference with sunlight penetration which disrupts photosynthetic activity in the aquatic system. Additionally, many synthetic dyes are toxic, carcinogenic, and resistant to biodegradation, which makes their removal a challenge [2].

Methyl violet is a commonly used synthetic cationic dye, used as a coloring agent in many industrial processes, as well as being a pH indicator. Even at low concentrations, Methyl Violet is associated with harmful biological effects, such as mutagenicity, carcinogenicity, and cytotoxicity. Its persistence in water bodies cause its accumulation which leads to biohazard risks to both aquatic ecosystem and human health. Therefore, the effective removal of Methyl Violet from wastewater before discharging it is essential [3, 4].

There are numerous methods that have been developed to remove dyes from wastewater, whether physical, chemical, or biological. Including, advanced oxidation processes, coagulation- flocculation, microbial degradation, and membrane filtration. However, many of these techniques have limitations such as high operational costs, energy intensity, generation of secondary pollutants, and reduced efficiency at low dye concentrations [5].

Adsorption, however, has emerged as one of the most efficient environmentally friendly methods, with many advantages like cost-effectiveness, simplicity, high efficiency even at low concentrations, and the potential for regeneration and reuse of the adsorbent [6].

In this context, nanoparticles have gained attention as quite advanced adsorbents because of the characteristics such as abundant active sites, also the unique chemistry of their surface, and of course their exceptionally high surface area compared to volume. Dye molecules interact more with such properties, leading to superior bulk counter parts occur. Materials of nano-structure enable tunable surface properties. These properties do allow for selective dye removal as well as potential regeneration [7].

Magnesium Oxide (MgO) nanoparticles, in particular, stand prominent as a good dye removal adsorbent. Since MgO is a non-toxic material that is thermally stable and inexpensive with a highly basic surface, therefore it is especially effective in the adsorbing of acidic dyes and cationic dyes like Methyl Violet. MgO exhibits improved surface area, porosity, and reactivity. When synthesized at the nano-scale, it results improved adsorption efficiency. MgO nanoparticles are promising candidate for

*Corresponding Author: Email: dr.mohammed@kecbu.uobaghdad.edu.iq

applications in wastewater treatment. Ease of synthesis coupled with chemical durability defines these characteristics [8-10].

MgO nanoparticles have also been used in earlier studies to adsorb synthetic dyes Methylene Blue, Rhodamine B, and Congo Red from the aqueous solution, and a high surface basicity and porosity as well as fast adsorption kinetics of the adsorbent have been credited as the prominent driving factors for the high affinity of adsorption [11, 12].

MgO nanoparticle synthesis methods explored by researchers include sol-gel, hydrothermal, combustion, and co-precipitation techniques. The oxalate co-precipitation method among them is a particularly attractive one. The process eases creation of MgO particles that are fine plus uniform showing better surfaces. It is cost-effective as well as scalable; furthermore, it is suitable enough for nanoparticle production with desirable morphological characteristics [13, 14].

Organic sorbents include natural clays and activation products from biomass (biochars and activated carbons) and other waste products, and many adsorbents tested show good removal efficiencies for Methyl Violet. However, these adsorbents may have low adsorption capacities, be too expensive, be difficult to separate or regenerate, or have low efficiencies under certain conditions. These limitations require the development of adsorbents that are highly efficient, inexpensive, and easily reusable [15, 16].

This study aims to use oxalate co-precipitation technique to synthesize MgO nanoparticles and test their adsorptive efficiency in the removal of Methyl Violet dye from aqueous solutions. Then, analyze and compare its performance with other nanomaterials to evaluate the potential of using MgO in wastewater treatment applications.

2- Materials and methods

2.1. Materials

For the preparation of magnesium oxide nanoparticles, magnesium sulfate heptahydrate ($MgSO_4.7H_2O$) from Sigma-Aldrich (Germany) was used as the magnesium precursor. Oxalic acid dihydrate ($H_2C_2O_4.2H_2O$) from Merck (Germany), serving as the precipitating agent. Hydrochloric acid (HCl, Merck, Germany) and sodium hydroxide (NaOH, Merch, Germany) were employed to adjust and control pH values during the synthesis and the adsorption experiments.

Methyl violet (MV), a synthetic cationic dye, purchased also from Merck was selected as the target adsorbate, it was used to prepare the aqueous solutions by dissolving it in distilled water. All the experiments were performed using freshly prepared solutions.

2.2. Synthesis of magnesium oxide (MgO) nanoparticles

MgO nanoparticles were prepared using wet chemical co-precipitation method, followed by thermal decomposition, a method widely used to produce oxide-based nanoparticles due to its cost effectiveness, and simplicity [17].

The nanoparticles were prepared by preparing 1.0 M solution of $MgSO_4.7H_2O$ using deionized water under magnetic stirring. A stoichiometric oxalic acid dehydrate was added drop-wise into the magnesium sulfate solution with continuous stirring (400 rpm) at room temperature. After 20 minutes, a white precipitate of Magnesium oxalates dehydrate was formed [18].

The precipitate was collected by vacuum filtration, washed multiple times by distilled water to remove any excess ions, and then dried in a hot air oven at 100 °C for 12 hours.

A calcination process was carried out in a muffle furnace at 700°C for 4 hours to obtain MgO crystalline nanoparticles. This temperature was based on prior studies suggesting that pore development and surface area are both enhanced at elevated thermal treatment [19].

2.3. Preparation of methyl violet solutions

The methyl violet dye stock solution was prepared by dissolving 0.1 g dye powder in 1 L of double distilled water in a volumetric flask. Then, different concentrations (20-50 mg/L) working solutions were prepared by diluting the stock solution. Those working solutions were placed in 100 ml amber glass containers to prevent degradation, as amber glass blocks most UV and visible light, which might affect of the light-sensitive dye.

2.4. Adsorption studies

Adsorption studies were performed in a batch manner following three consecutive sets to fully evaluate the performance of the MgO nanoparticles in the dye removal. The first set was prepared by mixing different weights of the magnesium nanoparticles (0.01-0.05 g/L) with variable dye concentrations (5-30 mg/L) of the methyl violet aqueous solution in 100 ml containers with initial pH of 3. The mixture was shaken by an orbital shaker (JSR Korea) at 200 rpm and room temperature. The equilibrium concentration of the dye was then measured by using UV-Vis Spectrophotometer (Shemadzu UV-1800, Japan) at a wavelength of 580 nm, which corresponds to maximum absorbance of MV dye [20]. This set was used to determine the best conditions in terms of contact time, and pH applying different pH (3-10) with 1 stepping each to determine the best pH. The second set of batch experiments was performed based on the best conditions of the first set, to determine the best adsorbent dosage.

The third set used the best conditions obtained from the previous two sets to study the effect of temperature variation applying different temperatures (20–50 °C) with

10 °C stepping to determine the best temperature that results the best removal efficiency.

The percentage of removal efficiency and the adsorption capacity at equilibrium (q_e) were calculated as follows [20]:

$$removal\ \% = \left(\frac{C_o - C_e}{C_o}\right) * 100 \quad (1)$$

$$q_e = (C_o - C_e) * \frac{V}{M} \quad (2)$$

Where, Co and Ce are the initial and equilibrium concentrations of the dye (mg/L), respectively. qe is the equilibrium dye concentration on adsorbent (mg/g). V is the volume of dye solution (L), and M is the mass of adsorbent (g).

3- Results and discussions

3.1. Scanning electron microscopy analysis (SEM)

Fig. 1 (a, b) explains the SEM micrographs of the MgO nanoparticles derived from wet chemical co-precipitation method and thermal decomposition at 700 °C show the characteristic morphological features confirming nano-sized MgO particle formation. As seen from Fig. 1 (a) (20.0 kx magnification), the particles are porous, irregular, and agglomerated loosely. Particle diameters are in the range of 65 nm to 156 nm, but most of the particles are in the range of 65–85 nm, although some larger aggregates up to 156 nm are observed. This is perhaps due to differences in nucleation and growth in the thermal decomposition reaction. The clustering obvious in the images is a result of the high surface energy and electrostatic attraction of MgO nanoparticles, favoring sticking of particles together during drying and calcination steps. Although individual particles are nanometer in size, the agglomerates are secondary agglomerates comprising an agglomeration of a network of interconnected pores. Fig. 1 (b), at 10.0 kx magnification, shows a larger view that identifies clusters with highly porous texture, suitable for catalytic as well as adsorption applications. The porosity arises because of the decomposition of magnesium oxalate on calcination, and the evolution of CO and CO_2 gases enables the formation of pores and enhances surface roughness. Such structure enhances available surface area and accessibility of active sites. Calcination temperature used (700 °C) is significant in achieving complete phase change of magnesium oxalate to magnesium oxide (MgO) with retention of crystallinity. Partial sintering, with some formation of larger particles and moderate decrease of overall surface area, can take place to some extent at this temperature. Control of particle growth and improvement of uniformity can possibly be achieved by, for example, optimization of the calcination conditions or using surfactants to control the growth.

The SEM analysis suggests that the synthesis process yields MgO nanoparticles that have nanoscale dimension, porous structure, and high surface heterogeneity, making them highly suitable for applications such as adsorption-based wastewater treatment. The synergy of reduced particle size and interconnected porosity achieves a best compromise between structural strength and surface area.

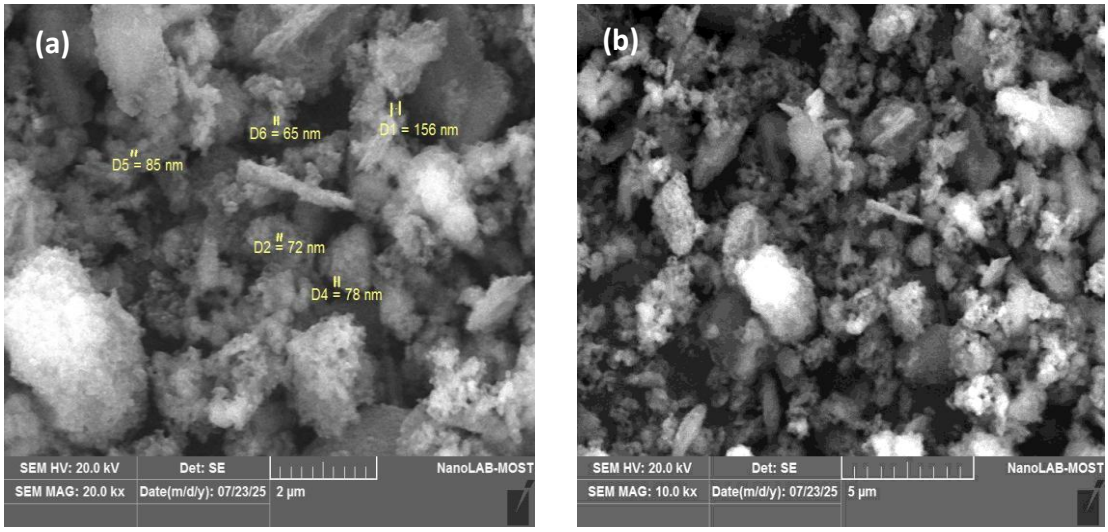

Fig. 1. (a) SEM of MgO nanoparticles (20.0 kx magnification), (b) SEM of MgO nanoparticles (10.0 kx magnification)

3.2. Atomic force microcopy analysis (AFM)

Atomic force microscopy (AFM) was used for the determination of the MgO nanoparticle topography before the adsorption of the organic dye. Analyzing the height image of a scan area of 2 × 2 µm in Fig. 2 provides information on a nano-granular topography with closely packed MgO nano-particles that form agglomerates. Large height variations (0–900 nm) suggest the presence of multi-particle agglomerates as well as individual particles, as is typically seen in precipitate-calcined MgO with strong particle interactions.

From AFM image analysis, the particle size distribution in Fig. 3 shows a wide distribution of particles in the nanometer range, which varies between 5 and 80 nm. However, the most dominant size range is between 10–20

nm. Given that 213 particles were analyzed, the mean particle size is estimated to be 40 ± 10 nm. This shows that there is a distribution of both primary nano-sized particles, as well as aggregated nano-domains.

Such nano-scale roughness, as well as a wide distribution within the particle size as shown in Fig. 4, is ideal for adsorption purposes.

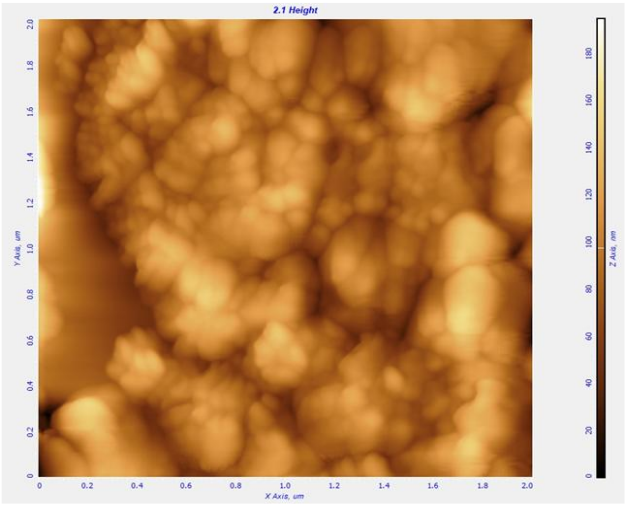

Fig. 2. AFM size distribution image of MgO nanoparticles over a 2 × 2 µm scan area

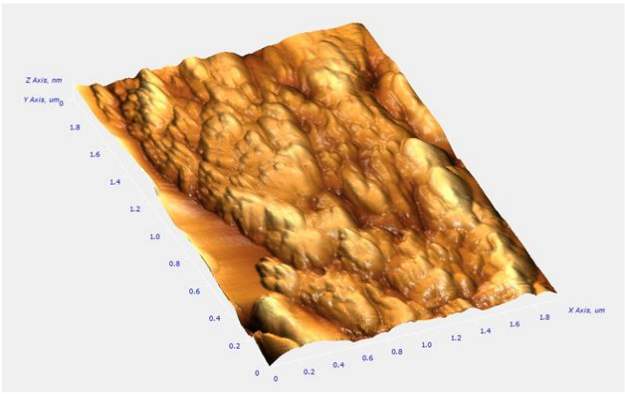

Fig. 3. 3D AFM height/topography image of MgO nanoparticles over a 2 × 2 µm scan area

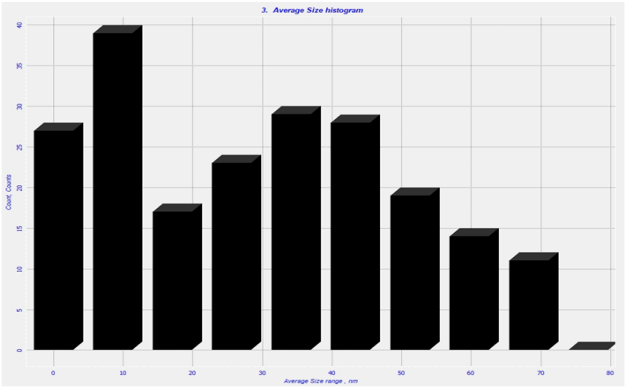

Fig. 4. Particle-size distribution histogram obtained from AFM analysis (n ≈ 213). The particle sizes range from ~5 to 80 nm, with an average size of 40 ± 10 nm and a dominant peak at 10 nm

3.3. X-ray diffraction analysis (XRD)

XRD pattern of the crystal structure of as-synthesized MgO nanoparticles is shown in Fig. 5 The pattern illustrates well-resolved and sharp diffraction peaks at 2θ positions of 36.77°, 42.77°, 62.14°, 74.55°, and 78.49°, respectively, corresponding to the (111), (200), (220), (311), and (222) planes of cubic periclase MgO (JCPDS card No. 45-0946), respectively. Observation of these reflections confirms the synthesis of phase-pure crystalline MgO with a face-centered cubic (FCC) structure.

The intensity of the (200) peak at 42.77° is very high and it suggests preferred orientation along this crystallographic direction, the unusually strong (200) peak means that many MgO crystallites are aligned so that their (200)/(100) planes are predominantly exposed to the X-ray beam. This "preferred orientation" does not change the cubic crystal structure but indicates anisotropic growth, where crystals develop more rapidly along particular directions. As a result, certain facets -here the {100} family- are more abundant, which can influence surface reactivity and adsorption behavior. There is no other peak for intermediate or secondary phases such as magnesium hydroxide or carbonates indicating the absence of any intermediate or secondary phase. This ensures that calcination temperature of 700 °C was sufficient for complete transformation of the precursor to desired oxide phase without decomposition by-products.

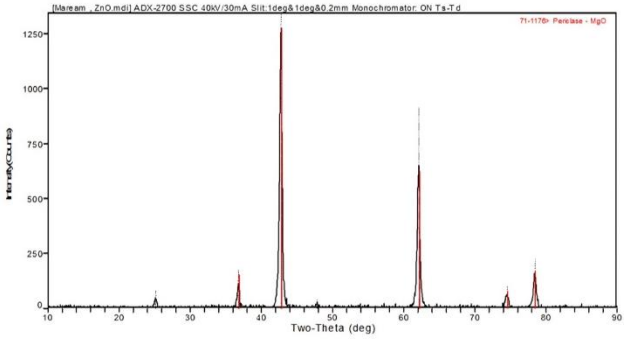

Fig. 5. XRD chart of MgO nanoparticles

Size of MgO nanoparticles was estimated from the Scherrer equation, full width at half maximum (FWHM) of the primary peaks. The Scherrer equation can be written as [21]:

$$\tau = \frac{K\lambda}{\beta \cos\theta} \quad (3)$$

where: τ is the average size of the (crystalline) domains, its value is smaller or equal to the crystalline size; K is a dimensionless shape factor, with a value close to unity.

The shape factor has a typical value of about 0.9, but varies with the actual shape of the crystallite; λ is the X-ray wavelength; β is the line broadening at half the maximum intensity (FWHM), after subtracting the instrumental line broadening, in radians. This quantity is also sometimes denoted as Δ(2θ). θ is the Bragg angle.

The crystallite size calculated was 19-30 nm, confirming the nanosize of the fabricated particles. The widths of the peaks were fairly thin, and the high intensity of peaks also indicate a well-crystallized phase with no lattice distortion or internal strain.

Overall, the XRD analysis confirms that the utilized co-precipitation after thermal decomposition process gave single-phase highly crystalline MgO nanoparticles of the requisite nanoscale sizes suitable for applications such as dye adsorption for which surface area and crystallinity are the deciding factors.

3.4. Effect of contact time

The effect of contact time when MgO nanoparticles are used as an adsorbent to remove methyl violet is illustrated as shown in Fig. 6.

The dye removal increased rapidly in the first 40 minutes, followed by a slower rate approaching equilibrium where the efficiency was about 68% at 60 minutes of contact time.

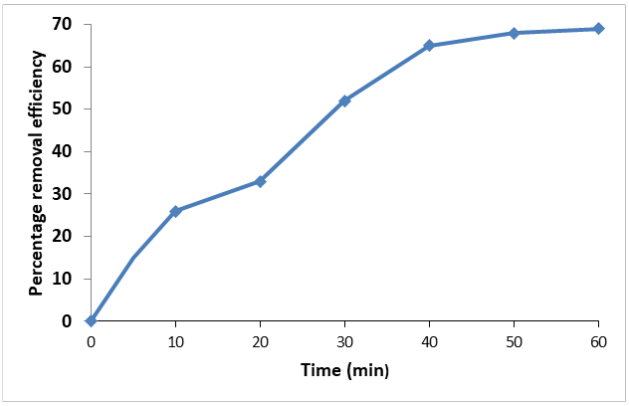

Fig. 6. The effect of contact time on the percentage of methyl violet dye removal (Co=50 mg/L, dosage =0.05 g, pH=3)

This adsorption pattern is characteristic for many adsorbents [22, 23], in the initial 30 minutes the adsorption rate was high due to the abundance of the unoccupied surface sites, and the strong gradient between these adsorbent sites and the dye molecules in the solution. As the process progresses, these sites were being increasingly occupied, causing the driving force for the mass transfer to be diminished and the repulsive forces between the dye molecules to hinder the further uptake from the bulk solution. The slowing of the rate means that the system is nearing the saturation. This behavior is consistent with the pseudo-second order kinetics suggesting valence forces involved in the chemisorption to be the dominant mechanism in this process [24]. Determining such effect while the system establishes equilibrium is crucial in the design of any continues batch wastewater treatment system.

3.5. Effect of pH

The effect of the solution's pH on the removal percentage is shown in Fig. 7 The percentage of dye removal reached its peak (~96%) at pH 6. At low pH values, there was an excess of free hydrogen ions (H^+), those positive ions were competing with the cationic dye molecules to occupy the available active sites on the adsorbent surface reducing the dye uptake as the nanoparticles surface becomes protonated causing the dye molecules to rebel the positively charged dye molecules [25].

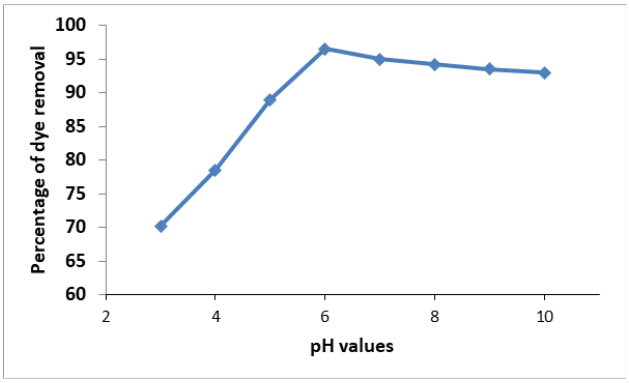

Fig. 7. The effect of pH on the percentage of methyl violet dye removal (Co=50 mg/L. dosage=0.05 g, t=60 min.)

At high pH values (neutral and basic conditions), the cationic dye molecules tend to transform into neutral form, which weakens the electrostatic attraction and limits the adsorption. A behavior that aligns with the Zeta potential studies [26]. This emphasizes the importance of pH optimization to obtain the best removal efficiency.

3.6. Effect of adsorbent dosage

The effect of MgO nanoparticles dosage when used to remove methyl violet dye is represented in Fig. 8 as follows:

The dosage range increased from 0.01 g/L to 0.06 g/L with 0.01 g/L step, the efficiency kept increasing with the increase of the adsorbent dosage starting from 66% at 0.01 g/L, until reaching the highest efficiency of 96% at 0.05 g/L.

The increase in the adsorbent dosage means that more adsorbent is introduced to the solution, increasing the available active binding sites on the MgO surface. With more surface area and more functional groups available for interaction, more dye molecules are going to be effectively adsorbed [27].

An increased adsorbent-to-dye ratio reduces the concentration of dye per unit mass of the adsorbent making it more probable for the dye molecules to encounter with active sites on the adsorbent [24].

However, at a certain point the increase in dosage may not result an increase in the removal efficiency, due to saturation effects, potential particle aggregation, and overlapping active sites [25]. To investigate this an

additional test was added to the set (0.06 g/L) giving a percentage of approximately (97%). Further study of the best dosage required for the best removal efficiency with consideration of cost effectiveness and the dye concentration in the aqueous solution should be made to prevent the wastage of adsorbent material.

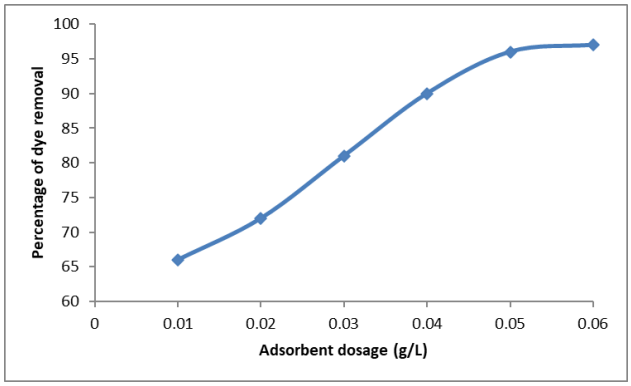

Fig. 8. The effect of adsorbent dosage on the percentage of methyl violet dye removal (Co=50 mg/L, t=60 min., pH=6, dosage=0.06 g/L)

3.7. Effect of temperature

The effect of temperature increase on the removal efficiency of dye molecules is shown on Fig. 9. The temperature was increased from 20 °C to 50 °C by a 10 °C step. The removal percentage decreased from ~ 96% at 20 °C to ~ 81% at 50 °C, which indicates that the adsorption process is exothermic. The dye molecules and the adsorbent surface interacted most likely due to lower temperatures. Chemisorption or electrostatic attraction governed the process. When temperature increases, kinetic energy of the dye molecules increases along with interaction forces weakening so partial desorption becomes possible.

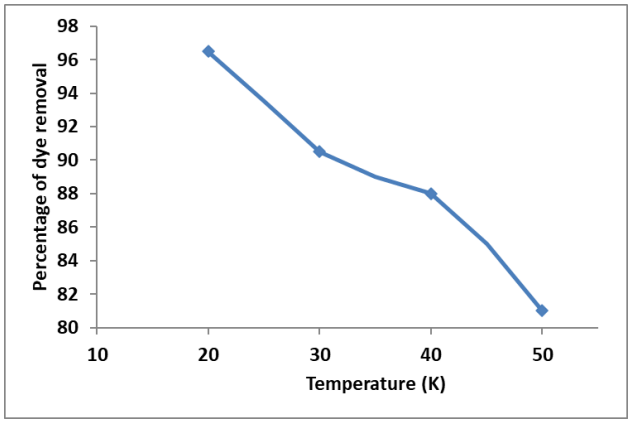

Fig. 9. The effect of temperature variation on the percentage of methyl violet dye removal (Co=50 mg/L, t=60 min, pH=6, dosage=0.05g)

Efficiency of removal might well be further reduced at high temperatures that could disrupt the structure of the adsorbent or change the chemistry of the surface. This trend underscores the sensitivity to the adsorption process nature, and it presses the need for a thorough thermodynamic study to quantify enthalpy (ΔH), Gibbs free energy (ΔG), and entropy (ΔS) changes to investigate the feasibility of adsorption under varying thermal conditions whether being different climates or industrial settings [23].

3.8. Adsorption isotherm insight

To evaluate and describe the equilibrium relationship between the adsorbate concentration and the amount adsorbed on the solid surface at a constant temperature, adsorption isotherms are crucial. The isotherms provide insight of the adsorbent capacity, surface properties, and the mechanism of adsorption.

For this insight two commonly used models in adsorption studies are going to be used and discussed, the Langmuir and Freundlich isotherms.

a. Langmuir isotherm model

The Langmuir isotherm is used to describe homogeneous monolayer adsorption, where the surface is uniform and the adsorption sites are finite.

The model is expressed as follows [23]:

$$qe = \frac{qmax*KL*Ce}{1+(Ce*KL)} \quad (4)$$

$$\frac{Ce}{qe} = \frac{1}{(qmax*KL)} + \frac{Ce}{qmax} \quad (5)$$

Where: q_e: equilibrium adsorption capacity (mg/g); C_e: equilibrium concentration (mg/L); q_{max}: maximum adsorption capacity (mg/g); K_L: Langmuir constant (L/mg).

From Langmuir linear plot (C_e/q_e vs. C_e), in Fig. 10, the slope is 0.012 with q_{max} is 83.3 mg/g. and KL is 1.2 L/mg Resulting R^2 value of 0.9931, which means that this system is an excellent fit with this model.

The experimental data showed a strong fit with this model, with a high regression coefficient (R^2) and a maximum monolayer adsorption (q_{max}) of 83.3 mg/g, the Langmuir constant (K_L) was determined to be 1.2 L/mg which indicates high affinity between the MgO nanoparticles surface and the methyl violet molecules [24].The dimensionless separation factor (RL) then can be calculated as follows:

$$RL = 1 / (1 + KL * C0) \quad (6)$$

Using the calculated values and the initial concentrations of the dye that were used in the study (10-50 mg/L), RL values ranged between 0.016 and 0.077, confirming the favorable adsorption.

b. Freundlich isotherm model

Freundlich model indicates heterogeneous adsorption and molecules overlapping on a non-uniform surface.

The model is expressed as follows [16, 19]:

$$qe = KF * Ce^{1/n} \quad (7)$$

$$log\ qe = log\ KF + (1/n) * log\ Ce \quad (8)$$

Where: q_e: equilibrium adsorption capacity (mg/g); Ce: equilibrium concentration (mg/L); KF: Freundlich adsorption coefficient (mg/g).

From the Freundlich linear plot, the slope (1/n) is -0.3, indicating poor model fit, and R^2 less than 0.95, which makes it less fit than the Langmuir model.

Fig. 11 and Table 1 demonstrates the results of both isotherms, clearing how the data does not fit with the Freundlich model which further confirms the mono-layered adsorption [24].

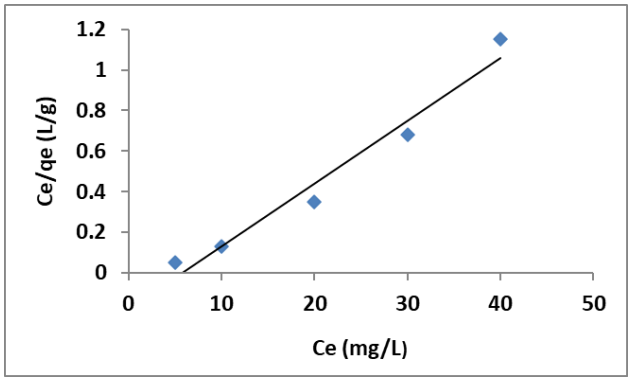

Fig. 10. Langmuir isotherm linear plot of the adsorption of methyl violet dye

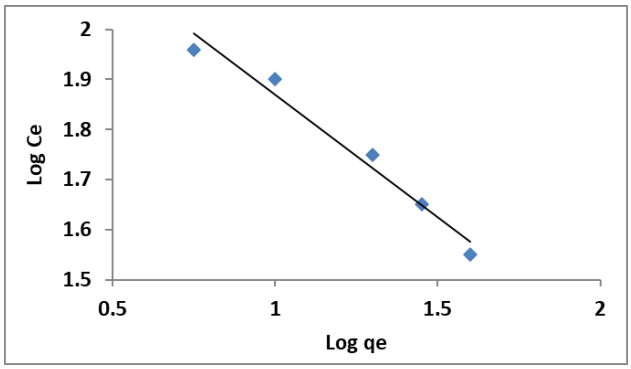

Fig. 11. Freundlich isotherm linear plot of the adsorption of methyl violet dye

Table 1. Isotherm model parameters values comparison

Isotherm Model	Parameter	Value	Unit	Interpretation
Langmuir	qmax	83.3	mg/g	Maximum monolayer adsorption capacity
Langmuir	KL	1.2	L/mg	Stronger affinity indicates favorable adsorption
Langmuir	R^2	0.9931	–	Excellent fit to experimental data
Langmuir	RL (Co = 10–50)	0.077–0.016	–	Favorable adsorption (0 < RL < 1)
Freundlich	KF	–	–	Not meaningful due to model inapplicability
Freundlich	1/n	-0.3	–	Negative value → physically invalid
Freundlich	R^2	0.92	–	Weaker fit compared to Langmuir

3.9. Adsorption kinetic insight

For further study of the kinetic behavior of adsorption process, the experimental results are being fitted into two models to find the best fit that describes the process properly (pseudo first order and pseudo second order). The linearized version of the equations is used to find the best fit and to properly describe each model.

a. Pseudo-first-order

The linearized equation for the Pseudo first order is [20, 23]:

$$Log\ (q_e - q_t) = log\ q_e - \left(\frac{k1}{2.303}\right) t \quad (9)$$

Where: q_e: adsorption capacity at equilibrium (mg/g); q_t: adsorption capacity at time t (mg/g); k_1: pseudo-first-order rate constant (1/min); t: contact time (min).

With C_o= 50 mg/l, V=0.1 L, M=0.05 g, Accordingly, k1=0.0857 min^{-1}, and R2~0.9583 which indicate nonphysical qt predictions.

PFO equation suggests that the adsorption rate is proportional to the number of unoccupied sites. Since the data doesn't fit with the model, this indicates that the process is not dominated by simple physical adsorption. The fitted data is shown in Fig. 12.

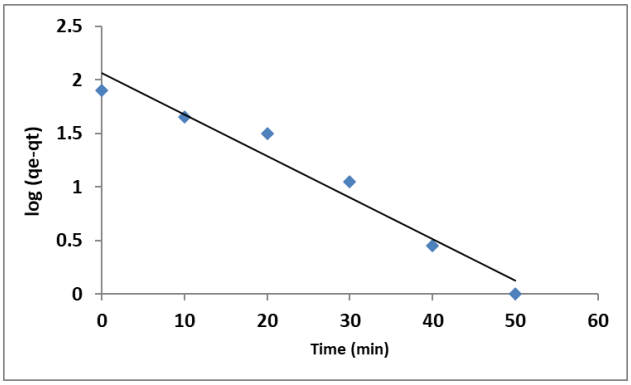

Fig. 12. Linearized pseudo-first-order kinetic model for the adsorption of methyl violet dye via MgO nanoparticles

b. Pseudo second order

The linearized equation of the Pseudo-Second-Order is:

$$t/q_t = (1 / k_2 q_e^2) + (t/q_e) \quad (10)$$

Where: q_e: adsorption capacity at equilibrium (mg/g); q_t: adsorption capacity at time t (mg/g); k_2: pseudo-second-order rate constant (g/mg·min); t: contact time (min).

When applying the experimental results in the equation, k_2 value is 1.8 * 10^{-3} g/mg.min, this value results R^2 ~0.9968 which shows a great fit with this kinetic model [29].

Pseudo second order assumes that the adsorption rate depends on the square of the number of unoccupied sites, which relates to the fact that the adsorption is controlled by chemical bonding (chemisorption). The fitted date is shown on Fig. 13.

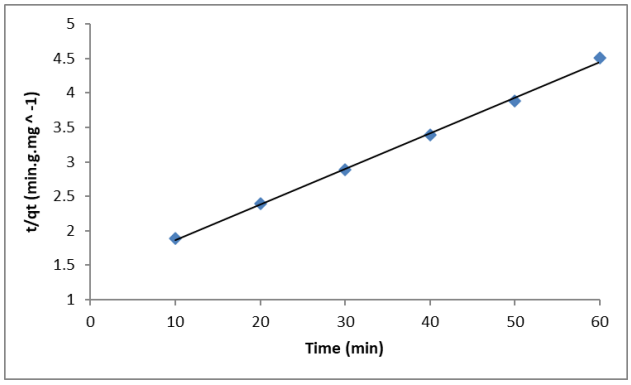

Fig. 13. Linearized pseudo-second-order kinetic model for the adsorption of methyl violet dye via MgO nanoparticles

4- Conclusion

MgO nanoparticles were synthesized through the oxalate co-precipitation method within a few steps. The XRD spectra established the presence of pure single-crystalline face-centered cubic structure MgO when calcinated at 700 °C, while SEM images described porous, irregularly shaped particles having a diameter in the range of 65–156 nm, and the AFM measurements indicated that these aggregates are composed of much smaller primary nanoparticles ranging from ~5 to 80 nm, with an average size of 40 ± 10 nm and a dominant peak at 10 nm. Best adsorption conditions were 0.05 g of MgO NPs, 50 mg/L methyl violet dye, pH 6, and contact time of 60 minutes. The adsorption data were fitted satisfactorily by the Langmuir isotherm model (R^2 = 0.9931) with q_{max} = 83.3 mg/g, and the kinetic study satisfactorily modeled a pseudo-second-order model (R^2 = 0.9968), indicative of chemisorption as the rate-controlling step. The results make MgO nanoparticles an affordable, prospective adsorbent for the removal of cationic dye from wastewater treatment. Aspects of optimizing MgO synthesis and surface area should be the initial focus for future studies, followed by experiments on the reusability and regenerability of the nanoparticles, adsorption of mixed dyes and actual industrial effluent, and scaling up to continuous treatment systems.

References

[1] D. A. Yaseen and M. Scholz, "Textile dye wastewater characteristics and constituents of synthetic effluents: A critical review," *International Journal of Environmental Science and Technology*, Vol. 17, No. 2, 2019, pp. 113–140. https://doi.org/10.1007/s13762-018-2130-z

[2] R. Al-Tohamy, S. S. Ali, F. Li, K. M. Okasha, Y. A.-G. Mahmoud, T. Elsamahy, H. Jiao, Y. Fu, and J. Sun, "A critical review on the treatment of dye-containing wastewater: Ecotoxicological and health concerns of textile dyes and possible remediation approaches for environmental safety," *Ecotoxicology and Environmental Safety*, Vol. 231, 2022. https://doi.org/10.1016/j.ecoenv.2021.113160

[3] Y. Shi, Z. Yang, L. Xing, X. Zhang, X. Li, and D. Zhang, "Recent advances in the biodegradation of azo dyes," *World Journal of Microbiology and Biotechnology*, Vol. 37, No. 8, 2021. https://doi.org/10.1007/s11274-021-03110-6

[4] B. Pizzicato, S. Pacifico, D. Cayuela, G. Mijas, and M. Riba Moliner, "Advancements in sustainable natural dyes for textile applications: A review," *Molecules*, Vol. 28, No. 16, 2023. https://doi.org/10.3390/molecules28165954

[5] M. Bilal, I. Ihsanullah, M. U. H. Shah, A. V. B. Reddy, and T. M. Aminabhavi, "Recent advances in the removal of dyes from wastewater using low-cost adsorbents," *Journal of Environmental Management*, Vol. 321, 2022. https://doi.org/10.1016/j.jenvman.2022.115981

[6] K. H. H. Aziz, F. N. Majeed, and M. K. Taib, "Advancements in application of modified biochar as a green and low-cost adsorbent for wastewater remediation from organic dyes," *Royal Society Open Science*, Vol. 11, 2024. https://doi.org/10.1098/rsos.232033

[7] N. S. Ali, N. M. Jabbar, S. M. Alardhi, H. Sh. Majdi, and T. M. Albayati, "Adsorption of methyl violet dye onto a prepared bio-adsorbent from date seeds: Isotherm, kinetics, and thermodynamic studies," *Heliyon*, Vol. 8, No. 8, 2022. https://doi.org/10.1016/j.heliyon.2022.e10276

[8] M. G. Ghoniem, F. A. M. Ali, B. Y. Abdulkhair, M. R. A. Elamin, A. M. Alqahtani, S. Rahali, and M. A. Ben Aissa, "Highly selective removal of cationic dyes from wastewater by MgO nanorods," *Nanomaterials*, Vol. 12, No. 6, 2022. https://doi.org/10.3390/nano12061023

[9] Z. Raji, A. Karim, A. Karam, and S. Khalloufi, "Adsorption of heavy metals: Mechanisms, kinetics, and applications of various adsorbents in wastewater remediation—A review," *Waste*, Vol. 1, No. 3, 2023, pp. 775–805. https://doi.org/10.3390/waste1030046

[10] P. Yadav, R. Saini, and A. Bhaduri, "Facile synthesis of MgO nanoparticles for effective degradation of organic dyes," *Environmental Science and Pollution Research*, Vol. 30, No. 28, 2023, pp. 71439–71453. https://doi.org/10.1007/s11356-022-21925-0

[11] M. G. Ghoniem *et al.*, "Highly selective removal of cationic dyes from wastewater by MgO nanorods," *Nanomaterials*, Vol. 12, No. 6, 2022. https://doi.org/10.3390/nano12061023

[12] H. Hegazey and E. A. Abdelrahman, "Efficient removal of methylene blue dye from aqueous media using magnesium borate/magnesium oxide ($Mg_3B_2O_6$/MgO) nanostructures," *Molecules*, Vol. 29, No. 14, 2024. https://doi.org/10.3390/molecules29143392

[13] T. S. Priya *et al.*, "Structural and optical properties of MgO nanoparticles synthesized by wet chemical route," *Journal of Materials Research and Technology*, Vol. 17, 2022, pp. 1–11.

[14] A. Muhaymin, H. E. A. Mohamed, K. Hkiri, A. Safdar, S. Azizi, and M. Maaza, "Green synthesis of magnesium oxide nanoparticles using *Hyphaene thebaica* extract and their photocatalytic activities," *Scientific Reports*, Vol. 14, No. 1, 2024. https://doi.org/10.1038/s41598-024-71149-0

[15] T. T. N. Nguyen *et al.*, "Enhancing methyl violet adsorption on sugarcane bagasse-based biochar via modification with sodium dodecyl sulfate," *Vietnam Journal of Catalysis and Adsorption*, Vol. 13, No. 4, 2024, pp. 26–31. https://doi.org/10.62239/jca.2024.069

[16] M. Alsuhybani *et al.*, "High removal of methylene blue and methyl violet dyes from aqueous solutions using efficient biomaterial byproduct," *Heliyon*, Vol. 10, No. 17, 2024. https://doi.org/10.1016/j.heliyon.2024.e36731

[17] H. Tahir, "Enhancement of adsorption and photocatalytic activity of MgO nanoparticles for the treatment of textile dye using ultrasound-assisted process by response surface methodology," *Desalination and Water Treatment*, Vol. 319, 2024. https://doi.org/10.1016/j.dwt.2024.100429

[18] V. N. Hegde *et al.*, "Effect of calcination temperature on structural, morphological, elastic and electrical properties of MgO nanoparticles synthesized by combustion method," *Journal of Physics and Chemistry of Solids*, Vol. 192, 2024. https://doi.org/10.1016/j.jpcs.2024.112071

[19] M. Sadiku *et al.*, "Removal of methyl violet from aqueous solution by adsorption onto halloysite nanoclay: Experiment and theory," *Toxics*, Vol. 10, No. 8, 2022. https://doi.org/10.3390/toxics10080445

[20] O. H. Fadhil *et al.*, "Adsorption of indigo carmine dye using corn leaves as natural adsorbent material," *Al-Khwarizmi Engineering Journal*, Vol. 17, No. 1, 2021. https://doi.org/10.22153/kej.2021.11.002

[21] A. D. Prasetya *et al.*, "X-ray diffraction profile analysis of pure ECAP-annealed nickel samples," *Journal of Physics: Conference Series*, Vol. 1436, 2020. https://doi.org/10.1088/1742-6596/1436/1/012113

[22] U.-S. B. Mahmood *et al.*, "Adsorption of eosin yellow dye by nickel oxide nanoparticles synthesized via oxalate co-precipitation method: Isotherm, kinetic and thermodynamic studies," *Physica Scripta*, Vol. 96, 2021. https://doi.org/10.1088/1402-4896/ac326e

[23] Z. R. Zair *et al.*, "Optimization, equilibrium, kinetics and thermodynamic study of Congo red dye adsorption from aqueous solutions using Iraqi porcelanite rocks," *Heat and Mass Transfer*, Vol. 58, No. 8, 2022, pp. 1393–1410. https://doi.org/10.1007/s00231-022-03182-6

[24] O. P. Murphy, M. Vashishtha, P. Palanisamy, and K. V. Kumar, "A review on the adsorption isotherms and design calculations for the optimization of adsorbent mass and contact time," *ACS Omega*, Vol. 8, No. 4, 2023, pp. 17407–17430. https://doi.org/10.1021/acsomega.2c08155

[25] H. Abdelmenim *et al.*, "Removal of cationic dyes from water using nano-adsorbents sulfonated carboxymethyl cellulose: Characterization, isotherm, kinetics and thermodynamics," *Port-Said Engineering Research Journal*, 2023. https://doi.org/10.21608/pserj.2023.195709.1223

[26] M. Yadav, S. Thakore, and R. Jadeja, "Removal of organic dyes using *Fucus vesiculosus* seaweed bioadsorbent: Equilibrium, kinetics and thermodynamic studies," *Environmental Chemistry and Ecotoxicology*, Vol. 4, 2022, pp. 67–77. https://doi.org/10.1016/j.enceco.2021.12.003

[27] İ. Uzun and F. Güzel, "Kinetics and thermodynamics of the adsorption of some dyestuffs and p-nitrophenol by chitosan and MCM-chitosan from aqueous solution," *Journal of Colloid and Interface Science*, Vol. 274, No. 2, 2004, pp. 398–412. https://doi.org/10.1016/j.jcis.2004.02.022

[28] M. ElKammah, E. Elkhatib, and M. Moubarak, "Effective elimination of indigo carmine in wastewater using green nanostructured modified biochar: Optimization, sorption equilibrium, kinetics, thermodynamics and mechanisms," *Applied Water Science*, Vol. 15, 2025. https://doi.org/10.1007/s13201-025-02556-5

[29] A. Gürses, K. Güneş, E. Şahin, and M. Açıkyıldız, "Investigation of the removal kinetics, thermodynamics and adsorption mechanism of Remazol Red RB using powder pumice," *Frontiers in Chemistry*, Vol. 11, 2023. https://doi.org/10.3389/fchem.2023.1156577

امتصاص صبغة الميثيل فيوليت باستخدام الجسيمات النانوية لأكسيد المغنيسيوم: التحضير والديناميكيات (الحركية)

محمد يعقوب عيسى [١،*]، مريم صالح المفتي [١]

١ قسم هندسة الكيمياء الاحيائية، كلية الهندسة الخوارزمي، جامعة بغداد، بغداد، العراق

الخلاصة

طريقة الترسيب المشترك بالأوكسالات (oxalate co-precipitation) بطريقة قابلة للتوسع لتحضير جسيمات نانوية من أكسيد المغنيسيوم (MgO). وكان المُرَسِّب المستخدم هو حمض الأكساليك (acid oxalic)، ومصدر المغنيسيوم القابل للذوبان هو كبريتات المغنيسيوم (magnesium sulfate). تم تحضير جسيمات MgO النانوية عالية البلورية عن طريق التحميص عند ٧٠٠°م، وتم توصيفها باستخدام حيود الأشعة السينية (XRD)، والمجهر الإلكتروني الماسح (SEM)، وتحليل المجهر القوي الذري (AFM). تم استخدام جسيمات MgO لدراسة امتصاص صبغة الميثيل فيوليت (MV) من المحاليل المائية تحت ظروف مختلفة تشمل زمن الاتصال، الرقم الهيدروجيني (pH)، تركيز الصبغة، ودرجة الحرارة. لوحظ أن أقصى امتصاص (٩٦٪) تحقق عند زمن ٦٠ دقيقة، pH = 6، درجة حرارة ٢٠°م، وجرعة الممتزِّب ٠.٠٥ جم/لتر. كما تبين أن تأثير درجة الحرارة عكسي بالنسبة لنسبة إزالة الصبغة ضمن النطاق المدروس (٢٠–٥٠°م). وصف نموذج الترتيب الزمني الزائف من الدرجة الثانية (pseudo-second-order, R^2=0.9968) ونموذج لانجمير (Langmuir, R^2=0.9931) التجارب الحركية وتجارب الإيزوثرم على التوالي، مما يشير إلى تغطية أحادية الطبقة وامتصاص كيميائي (chemisorption). وأثبتت النتائج أن قدرة امتصاص MgO أعلى مقارنة بالممتزّات المكافئة الأخرى (q_{max} = 83.1 mg/g).

الكلمات الدالة: الجسيمات النانوية لأكسيد المغنيسيوم (MgO)، صبغة البنفسجي الميثيلي، نماذج متساويات الامتزاز، حركيات الامتزاز.